ORNL/TM-2021/2192

Long-Term Thermal Aging Effect Evaluation for Grade 92 and 316L at The LWR Relevant Temperature

Lizhen Tan
Xiang Chen

September 2021

OAK RIDGE National Laboratory

ORNL IS MANAGED BY UT-BATTELLE LLC FOR THE US DEPARTMENT OF ENERGY

ORNL/TM-2021/2192

Light Water Reactor Sustainability (LWRS) Program
M3LW-21OR0406023

LONG-TERM THERMAL AGING EFFECT EVALUATION FOR GRADE 92 AND 316L AT THE LWR RELEVANT TEMPERATURE

Lizhen Tan, Xiang Chen
Materials Science and Technology Division

September 2021

Prepared by
OAK RIDGE NATIONAL LABORATORY
Oak Ridge, TN 37831-6283
managed by
UT-BATTELLE LLC
for the
US DEPARTMENT OF ENERGY
under contract DE-AC05-00OR22725

CONTENTS

LIST OF FIGURES

LIST OF TABLES

ACKNOWLEDGMENTS

This research was sponsored by the U.S. Department of Energy (DOE), Office of Nuclear Energy (NE), under the Light Water Reactor Sustainability (LWRS) Program.

The authors are grateful to Tom Geer of Oak Ridge National Laboratory (ORNL) for metallographic specimen preparation and optical microscopy imaging, Weicheng Zhong of ORNL for scanning electron microscopy, and Eric Manneschmidt and Jordan Reed of ORNL for the mechanical tests. Thomas M. Rosseel and Mikhail Sokolov of ORNL are also acknowledged for reviewing this report.

ABSTRACT

Life extension of the existing nuclear reactors imposes accumulated damages, such as higher fluences and longer periods of corrosion, to structural materials, which would result in significant challenges to the traditional reactor materials such as type 304 and 316 stainless steels. Advanced alloys with superior radiation resistance will increase safety margins, design flexibility, and economics for not only the life extension of the existing fleet but also new builds with advanced reactor designs. The Electric Power Research Institute (EPRI) initiated a collaboration with the Department of Energy (DOE) Light Water Reactor Sustainability (LWRS) Program on the Advanced Radiation Resistant Materials (ARRM) program, focused on developing and test degradation resistant alloys for light water reactor (LWR)-relevant environments. Based on a comprehensive microstructure and property screening, the ARRM program selected a total of five alloys (i.e., Grade 92, 310, 690, 718A, and 725), together with 316L and X-750 as references, for further investigations.

Because thermal aging could exert a synergistic effect on neutron irradiation due to the low neutron damage rate on the order of 10^{-7} displacements per atom per second (dpa/s), Grade 92 and two heats of 316L were selected for this task to study the effect of aging at 350°C for ~12.6 kh and ~37 kh on microstructure and mechanical properties. The two heats of 316L are differentiated by their differing amounts of δ-ferrite, i.e., ~1 vol% in heat T1103 and ~4% in heat N5B8. The two heats of 316L were subjected to 15% cold work (CW) as this condition is often used in nuclear reactors to help trapping radiation-induced defects and thus postpone the radiation-induced steady state swelling stage. The aging times approximately correspond to 5 dpa and 13 dpa neutron irradiation, respectively, which can serve as references for the irradiated alloy samples with the respective doses to help understand the independent neutron damage influence on microstructures and mechanical properties. Optical microscopy was used for microstructural characterization. Hardness, tensile, Charpy impact toughness, and fracture toughness in the ductile regime of the aged samples were examined.

Blocks of Grade 92 and two heats of 316L (T1103 and N5B8) were aged at 350°C for 12.6-12.7 kh and 36-37 kh. Metallographic samples, type SS-3 tensile specimens along the longitudinal direction, half-size Charpy V-notch specimens in the T-L orientation, and 0.2T or 0.25T compact tension fracture toughness specimens in the T-L orientation were machined from the aged blocks for the respective microstructural characterization and mechanical property evaluation. The ~12.6 kh aging results of Grade 92 and the two heats of 316L were reported in 2020. In general, the aging conditions did not result in noticeable microstructural changes under optical microscopy, except for some Laves phase in ~100–200 nm in Grade 92 under SEM.

The aging resulted in some reduction in hardness and yield/ultimate tensile strength with some increases in uniform and total plastic elongations for the 36 kh aged Grade 92. These effects may have increased the enhancement of Charpy impact toughness, e.g., ~56 J upper-shelf energy for the 36 kh aged condition compared with ~34 J for the 12.7 kh aged condition and ~30 J for the unaged condition. The fracture toughness of the 36 kh aged Grade 92 showed decent toughness of ~289 MPa$\sqrt{m}$ (K_{jq}) with ~102 tearing modulus at 22°C and ~209 MPa$\sqrt{m}$ with ~111 tearing modulus at 300°C, which slightly reduced the fracture toughness but slightly increased the tearing modulus due to the ~12.7 kh aged condition. The aging induced Laves phase did not have a noticeable influence on the mechanical properties.

Unlike the negligible or slightly increased hardness in the ~12.6 kh aged condition, the ~37 kh aging resulted in significant reductions in the hardness of 316L-T1103 and 316L-N5B8 samples. The ~37 kh aging also significantly reduced the standard deviations of the two 316L heats, suggesting that the longer aging time reduced the 15%CW induced inhomogeneity in the microstructures. The aging-induced hardness evolution is consistent with their yield strength changes. The shorter time (~12.6 kh) aging noticeably reduced the uniform and total plastic elongation while the longer time (~37 kh) aging

recovered the elongation to near the unaged condition of 316L-T1103. In contrast, the aging showed minor effects on the uniform and total plastic elongation of 316L-N5B8, with similar or lower elongations than the 316L-T1103 sample. In general, the fracture toughness and tearing modulus at 300°C tend to be lower than that at room temperature. The longer aged (~37 kh) samples at 350°C tend to have slightly reduced or negligibly influenced fracture toughness but have increased tearing modulus in general compared to the shorter aged (~12.6 kh) samples. The fracture toughness and tearing modulus of 316L-T1103 are significantly higher than that of 316L-N5B8. The results indicate that the presence of a high volume of δ-ferrite (316-N5B8) would noticeably impair fracture toughness although it may negligibly influence hardness and tensile properties. The fracture toughness and tearing modulus of Grade 92 are between those of the two 316L heats.

1. INTRODUCTION

Nuclear power currently provides a significant fraction of the United States' non-carbon emitting power generation. In future years, nuclear power must continue to generate a significant portion of the nation's electricity to meet the growing electricity demand, clean energy goals, and to ensure energy independence. New reactors will be an essential part of the expansion of nuclear power. However, given the limits on new builds imposed by economics and industrial capacity, the extended service of the existing light water reactor (LWR) fleets will also be required.

Nuclear reactors present a very harsh environment for components service. Components within a reactor core must tolerate high temperatures, water, stress, vibration, and an intense neutron field. With the nominal irradiation temperature of ~290°C in LWRs, the actual component temperatures range from 270°C to 370°C depending on the relative position of the component within the reactor core and relative amounts of cooling and gamma heating. Degradation of materials in this environment can lead to reduced performance, and in some cases, sudden failure. Extending the service life of a reactor will increase the total neutron fluence to each component and may result in radiation-induced effects not yet observed in LWR conditions, although this form of degradation has been observed in fast reactor conditions. Increases in neutron fluence may exacerbate radiation-induced or -enhanced microstructural and property changes. Comprehensive reviews on radiation effects on the traditional structural materials of LWRs can be found in Ref. [1,2,3].

It is clearly desirable to have advanced alloys that possess greater radiation resistance than the traditional reactor materials, while having satisfactory performance in other primary properties. The use of such advanced alloys in replacing the traditional reactor materials for the extension of the existing fleets and the building of new reactors will bring improved safety margins and economics. To identify and develop advanced radiation resistant materials, Electric Power Research Institute (EPRI) has partnered with the Light Water Reactor Sustainability (LWRS) Program of the Department of Energy (DOE) to conduct an Advanced Radiation Resistant Materials (ARRM) program. The EPRI report entitled of *Critical Issues Report and Roadmap for the Advanced Radiation-Resistant Materials Program* [4] reviewed the current commercial and advanced alloys that are applicable as LWR core structural materials and developed a detailed research plan to meet the goal of the program.

After comprehensive microstructure and property screening, the ARRM program [5,6,7,8,9,10] selected five alloys (i.e., Grade 92, 310, 690, 718A, and 725), together with 316L and X-750 as reference alloys, for further investigations. Thermal annealing is often considered to have a significant role on neutron irradiation results because of the low damage rate typically on the order of 10^{-7} displacements per atom per second (dpa/s). Therefore, thermal aging of Grade 92 and two heats of 316L were selected in this task to demonstrate the effect of aging at 350°C for ~12.6 kh and ~37 kh on the microstructures and mechanical properties of the two types of alloys. The aging times approximately correspond to 5 dpa and 13 dpa neutron irradiation, which can serve as references for the irradiated samples of the alloys to help understand the independent influence of neutron damage on microstructures and mechanical properties. The ~12.6 kh aging results of the two types of alloys were reported in the 2020 ARRM milestone report [11]. This report presents the ~37 kh aging results and compares them to the ~12.6kh aging results.

2. EXPERIMENTAL

2.1 ALLOYS

Grade 92 and 316L were selected in the aging study at 350°C. The compositions in weight percent (wt%) of the steels are listed in Table 1, together with the fabrication methods and specific heat treatments for the steels listed in Table 2. Two heats of 316L are included in the aging study, which are primarily differentiated by their δ-ferrite amounts. Following the ASTM A800/A800M-20, "Standard practice for estimating ferrite content of stainless steel castings containing both ferrite and austenite", the ratio of Cr_e/Ni_e = (Cr + 1.5Si + 1.4Mo – 4.99)/(Ni + 30C + 0.5Mn + 26(N – 0.02) + 2.77) gives 0.929 for heat T1103 and 1.017 for heat N5B8, corresponding to δ-ferrite amount of 0–3.5 vol% and 1.5–7 vol%, respectively. Therefore, we can roughly estimate that there is ~1 vol% δ-ferrite in heat T1103 while ~4 vol% δ-ferrite in heat N5B8 according to the guidance of the ASTM A800/A800M-20. The use of alloy 316L in LWRs is typically in the range of 15–20% cold work (CW) so as to increase irradiation defects trapping sites and thus postponing the occurrence of steady state swelling under neutron irradiation. Accordingly, 15% CW was applied in this study to the two heats of 316L.

Table 1. Vendor reported compositions (wt%) of Grade 92 and 316L with Fe as balance

Alloy	Heat	Cr	Ni	Mo	W	V	Nb	Si	Mn	C	N	P	S	Cu
Grade 92	011448	8.81	0.12	0.36	1.78	0.18	0.08	0.1	0.4	0.091	0.046	<0.005	<0.0005	<0.01
316L	T1103	17.5	12.3	2.3	-	-	-	0.46	1.8	0.022	0.06	0.027	0.001	0.2
316L	N5B8	16.66	10.01	2.00	-	-	-	0.31	1.43	0.014	0.05	0.032	0.0013	0.41

Table 2. Fabrication condition of Grade 92 and 316L

Alloy	Heat number	Fabrication method [a]	Heat treatment [b]
Grade 92	011448	VIM	1130°C/0.5h/WQ + 600°C/1h/AC + 750°C/4h/AC
316L	T1103	EAF	1050°C/0.5h/WQ
316L	N5B8	EAF, AOD, Continuous casting	>1038°C/WQ

[a] VIM – vacuum induction melting; EAF – electric arc furnace; AOD – argon oxygen decarburization
[b] AC – air cooling; WQ – water quenching

2.2 THERMAL AGING

Blocks of materials from the heats of Grade 92 and 316L were aged in a box furnace in an ambient atmosphere at 350°C for 12.7 kh and 36 kh for Grade 92 and 12.5 kh and 37 kh for 316L.

2.3 MICROSTRUCTURAL CHARACTERIZATION

Metallographic samples were prepared from the aged blocks of the materials, which were ground and polished to a mirror finish. The solution of $50H_2O/5HNO_3/1HF$ and Glyceregia etchant were used for Grade 92 and 316L, respectively, reveal their microstructures. Optical micrographs were taken from the etched Grade 92 and 316L samples. Scanning electron microscopy was used to characterize Laves phase in the aged Grade 92 samples.

2.4 MICROHARDNESS TEST

Vickers microhardness on the metallographic samples were measured using a 1 kgf load with 20 s dwell times. Five measurements were conducted on each sample to obtain statistical hardness results.

2.5 TENSILE TEST

Type SS-3 miniature specimens were machined from the aged blocks of the materials with the gauge length direction parallel to the rolling direction of the plates. Figure 1 shows the geometry of type SS-3 specimens. Tensile tests were conducted in air at temperatures ranging from room temperature up to 700°C, following the ASTM E8 "Standard test methods for tension testing of metallic materials" and E21 "Standard test methods for elevated temperature tension tests of metallic materials." Tests were performed using an MTS tensile testing system with a load cell possessing a 22 kN (5000 lbf) capacity, which is integrated in the load train. Tensile testing was performed at a crosshead speed of 0.018 in/min to achieve the nominal strain rate of 0.001 s^{-1}. The tensile testing system, load cells, and furnace thermocouples were routinely calibrated.

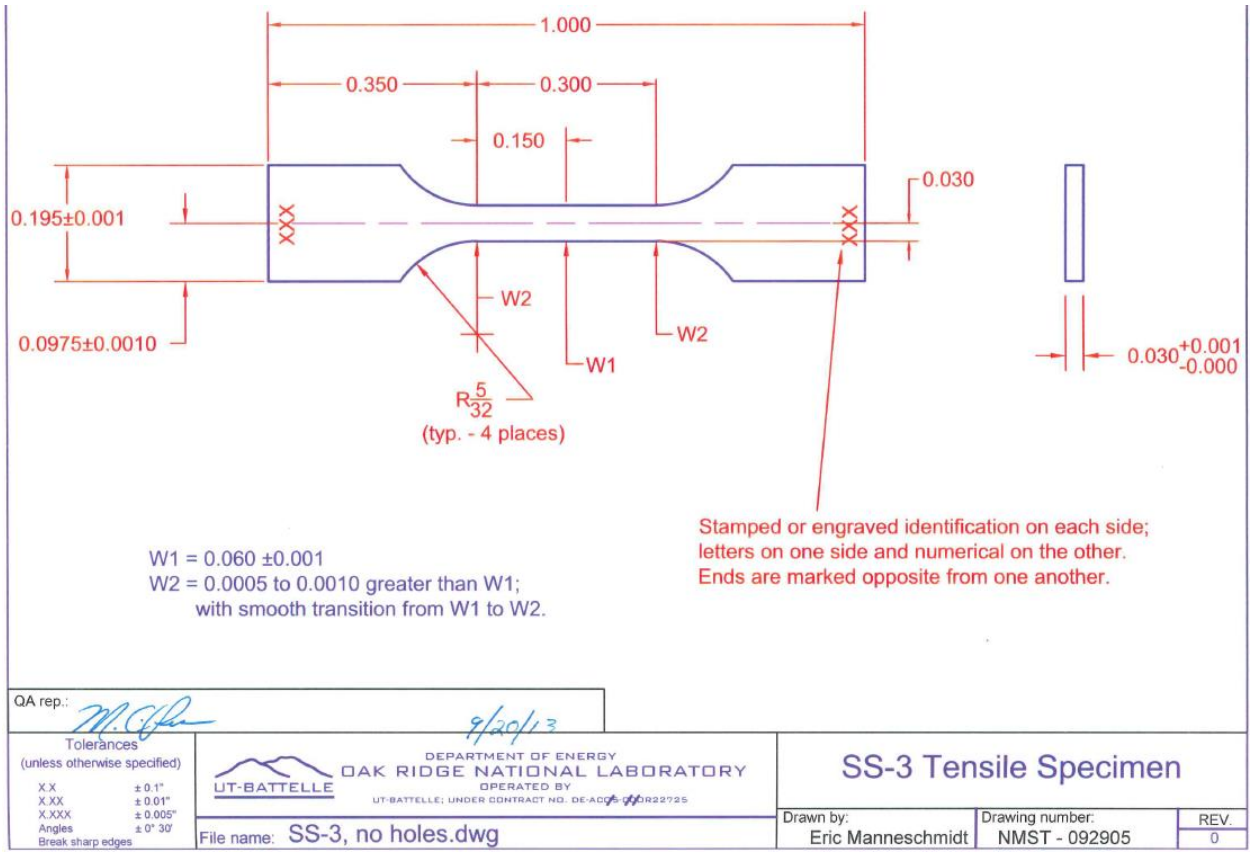

Figure 1. Geometry of type SS-3 miniature specimen in inch.

2.6 CHARPY V-NOTCH IMPACT TEST

Half-size Charpy V-notch specimens, with its geometry shown in Figure 2, were machined from the aged block of Grade 92 with the ligament under the V-notch in parallel with the longitudinal direction of the plates, i.e., the T-L (transverse-longitudinal) orientation. Charpy impact tests were conducted on a Tinius Olsen Charpy 300 ft-lb machine according to the ASTM E23-12c, "Standard test methods for notched bar impact testing of metallic materials." The measurement calibration of the Charpy machine is performed annually through testing of specimens with certified values to verify the accuracy of the machine. The half-size Charpy V-notch specimens were tested at temperatures ranging from –150°C to 100°C to measure the absorbed impact energies, e.g., upper-shelf energy (USE), and to determine the ductile-brittle transition temperature (DBTT) of the aged Grade 92.

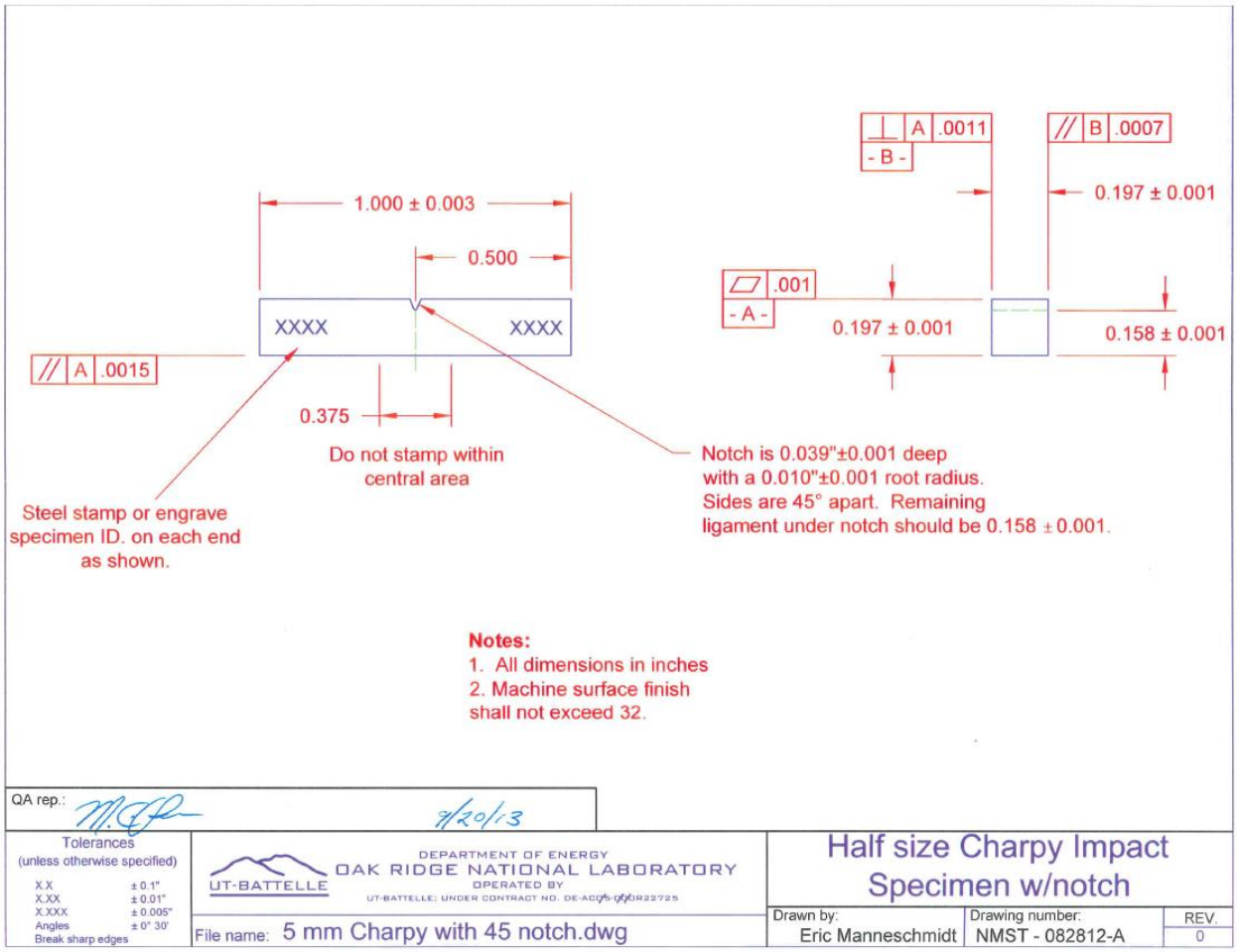

Figure 2. Geometry of half-size Charpy V-notch specimen in inch.

2.7 FRACTURE TOUGHNESS TEST

Compact tension specimens machined according to the specifications in Figure 3 for 0.2T and Figure 4 for 0.25T were extracted along the T-L orientation from the aged plates of Grade 92 and 316L, respectively. A total of six specimens per material were tested with a computer-controlled test and data acquisition system in accordance with the ASTM E1820, "Standard Test Method for Measurement of

Fracture Toughness," for the ductile regime at elevated temperatures (>~22°C). The specimens were fatigue pre-cracked to a ratio of the crack length to specimen width (a/W) of about 0.5 before fracture testing. Specimens were tested in the laboratory on a 98-kN (22-kip) capacity servo-hydraulic machine. All tests were conducted in displacement control, with an outboard clip gage having a central flexural beam that was instrumented with four strain gages in a full-bridge configuration.

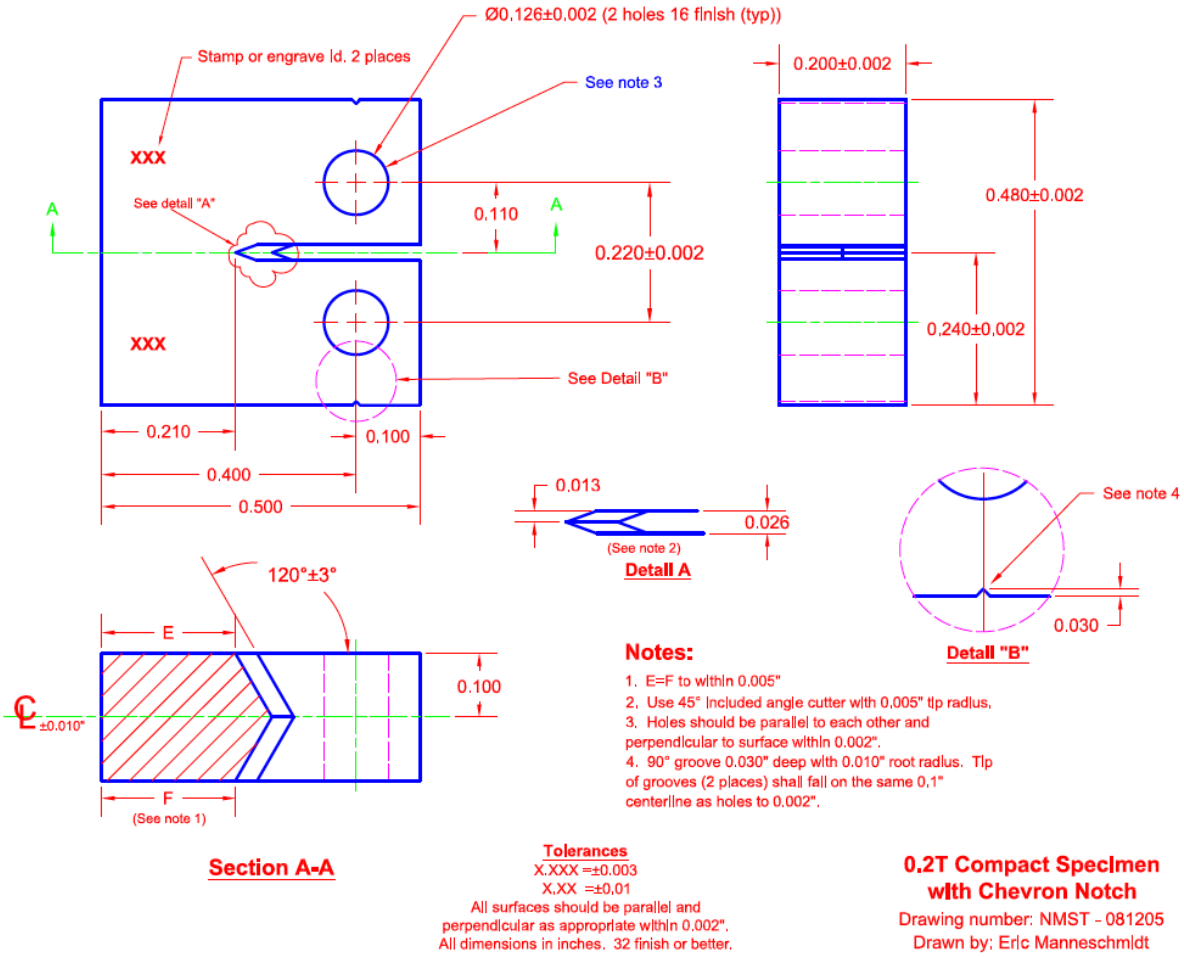

Figure 3. Specification of 0.2T compact tension specimen (dimensions are in inches).

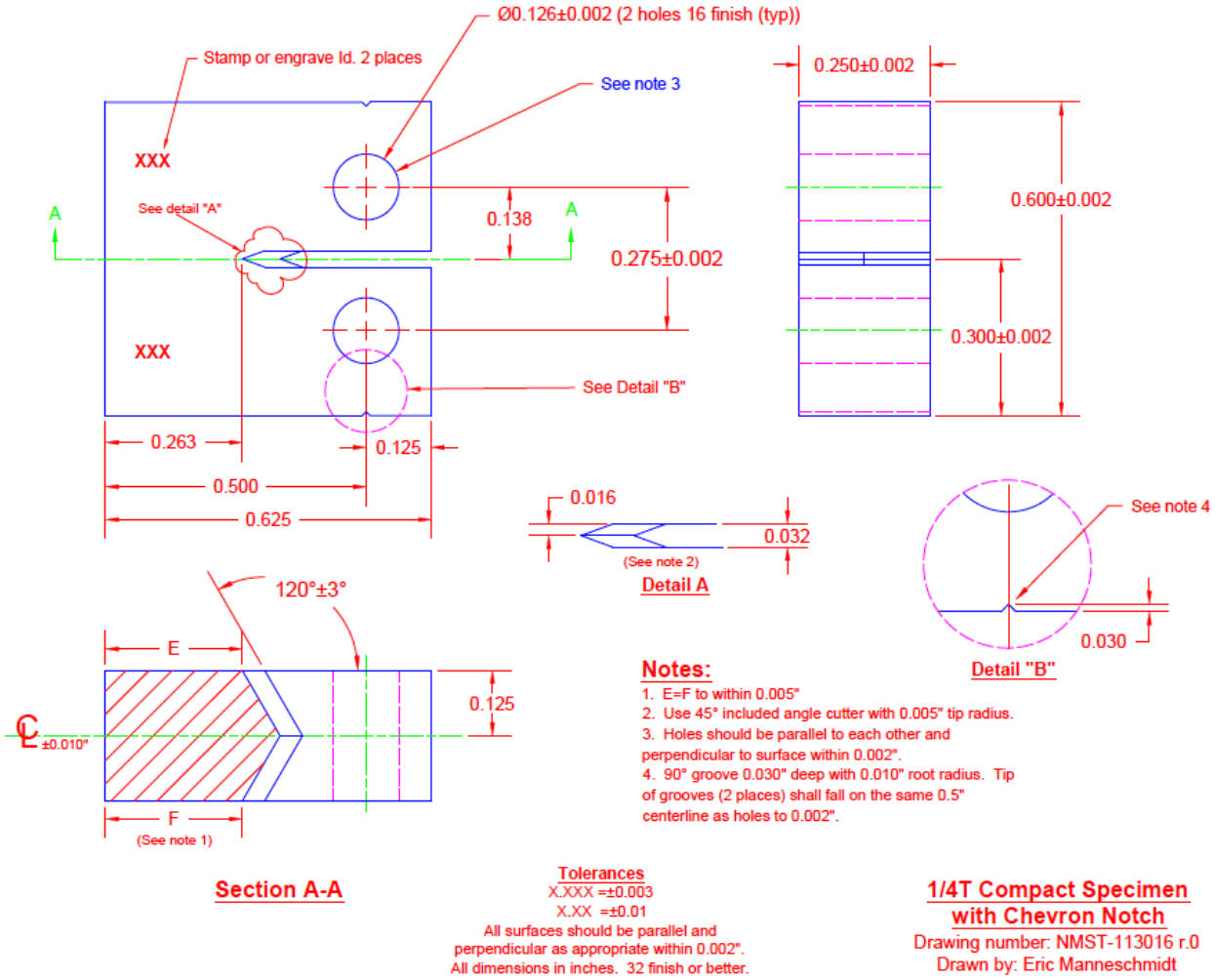

Figure 4. Specification of 0.25T compact tension specimen (dimensions are in inches).

3. AGING-INDUCED MICROSTRUCTURAL EVOLUTION

3.1 Grade 92 (Ht. 011448)

The microstructures of Grade 92 aged at 350°C for 12.7 kh and 36 kh are shown in Figure 5. The aging did not result in noticeable grain and lath structure changes to Grade 92. The backscattered electron images in Figure 6 show some small white precipitates primarily in ~100–200 nm, which primarily decorate the hierarchy boundaries, i.e., prior-austenite, packet, and block, except for lath, in ferritic-martensitic steels for both the shorter and longer time aged samples. The small white precipitates are rich in W with a high–Z to yield a high contrast under the backscattered electron images, which are believed to be Laves phase, e.g., Fe_2W. A few coarse white precipitates in ~400 nm, e.g., the one in Fig. 6a pointed by a white arrow, which are rich in Nb and believed to be MX (M=Nb, X=C/N) precipitates. The longer time aged sample (Fig. 6b) shows similar microstructures. A few black features were also observed in both shorter and longer time aged samples, with sizes as large as ~500 nm as shown in Fig. 6b, which may be inclusions or etched precipitate sites in the material. Among the microstructure features, only the Laves phase was induced by the aging.

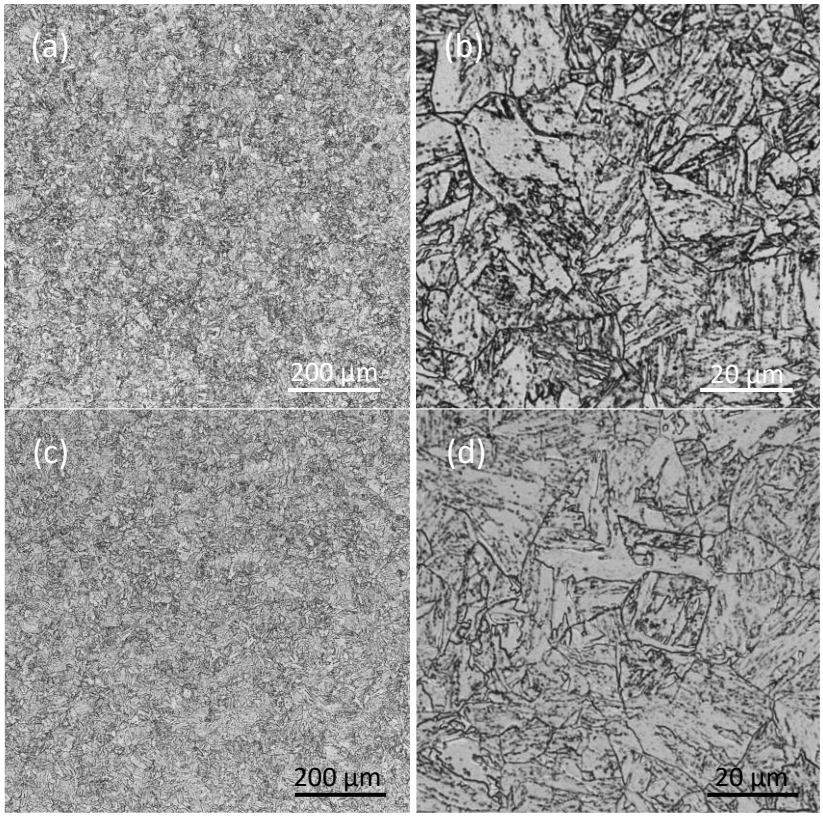

Figure 5. Optical images of Grade 92 aged at 350°C for (a-b) 12.7 kh and (c-d) 36 kh.

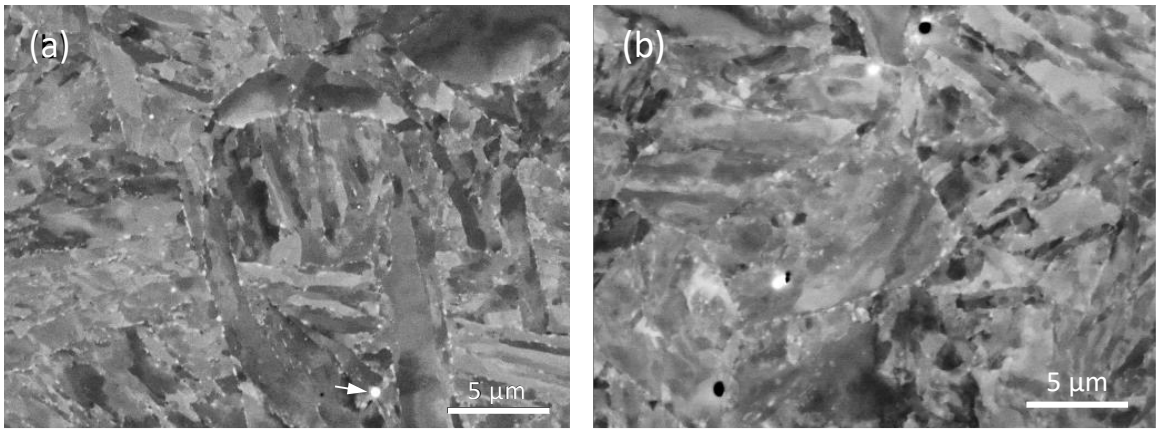

Figure 6. Backscattered electron images of Grade 92 aged at 350°C for (a) 12.7 kh and (b) 36 kh.

3.2 316L (Ht. T1103)

Figure 7 compares the optical micrographs of the 15%CW 316L heat T1103 (~1 vol% δ-ferrite) prior to aging with that of a sample aged at 350°C for 12.5 kh and 37 kh. A few short strings of δ-ferrite, e.g., those pointed by black arrows in Fig. 7a, are observable at some of the austenite grain boundaries in the 15%CW 316L sample prior to aging. The higher magnification micrograph in Fig. 7b indicates the presence of twins and some slip lines induced by the 15%CW. After the 12.5 kh and 37 kh aging, the grain structure with the presence of short strings, twins and slip lines were not noticeably changed. Some grains have extensive CW-induced slip lines as shown in Fig. 7f, which indicates inhomogeneity of this type of features that were not a result of the aging.

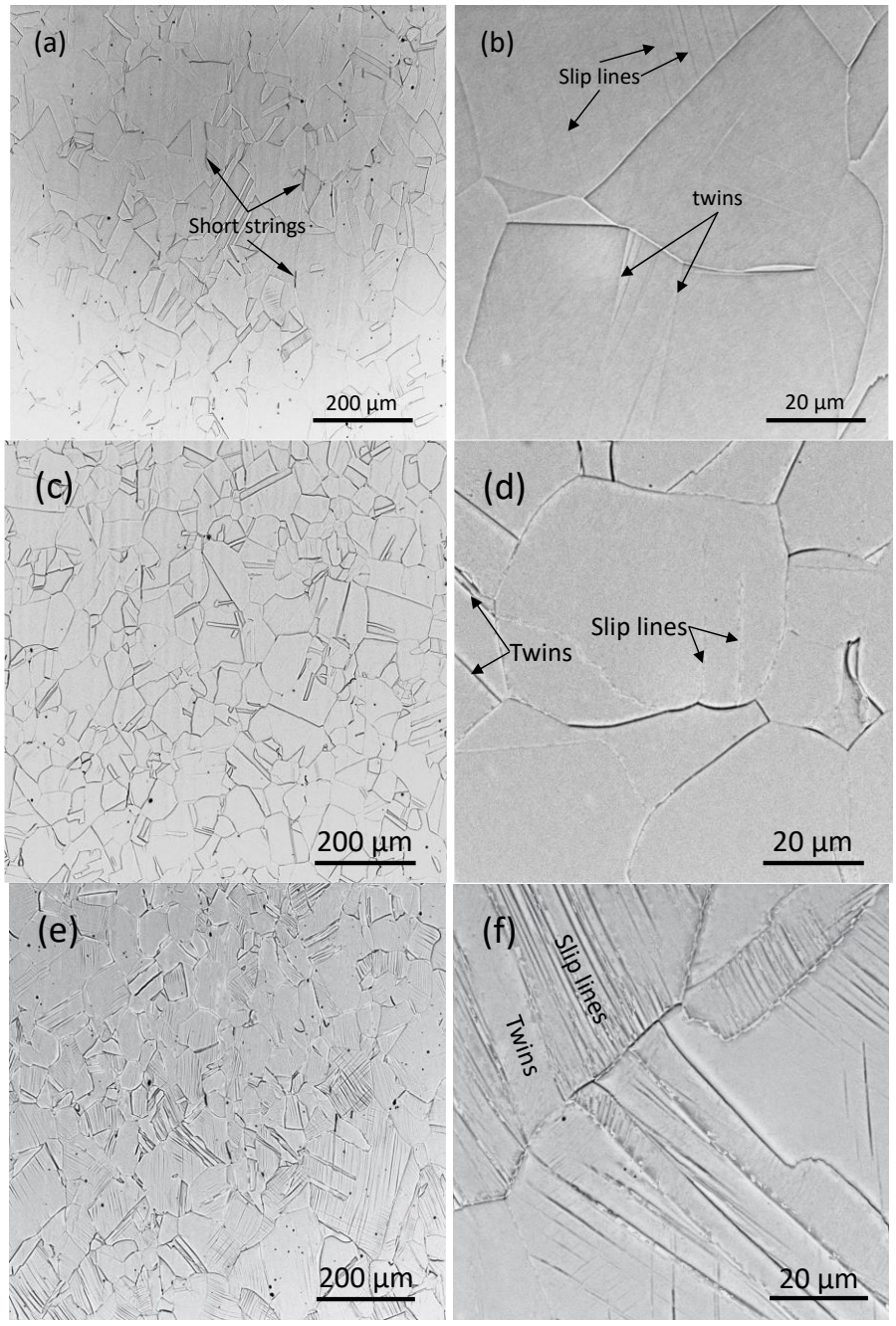

Figure 7. Optical micrographs of 15%CW 316L (T1103): (a-b) prior to aging and aged at 350°C for (c-d) 12.5 kh and (e-f) 37 kh.

3.3 316L (Ht. N5B8)

Figure 8 compares the optical micrographs of the 15%CW 316L heat N5B8 (~4 vol% δ-ferrite) prior to aging with that aged at 350°C for 12.5 kh and 37 kh. Two types of δ-ferrite, i.e., Widmanstätten and short strings pointed by black arrows in Fig. 8a, were observed in this heat of 316L prior to aging. The high magnification micrograph in Fig. 8b shows some slip lines induced by the 15%CW. It is not clear whether the small black features in Fig. 8b are inclusions or precipitates because of the etched surface. After the

12.5 kh and 37 kh aging, the grain structure with the presence of two types of δ-ferrite and slip lines was not noticeably changed. However, many long strings and primarily short strings of δ-ferrite are visible in Fig. 8c and Fig. 8e, respectively, which is not induced by the aging but indicates the inhomogeneous distribution of long and short strings of δ-ferrite in the heat of 316L. The high magnification micrographs in Fig. 8d and Fig. 8f show slip lines from the 15%CW and the two types of δ-ferrite.

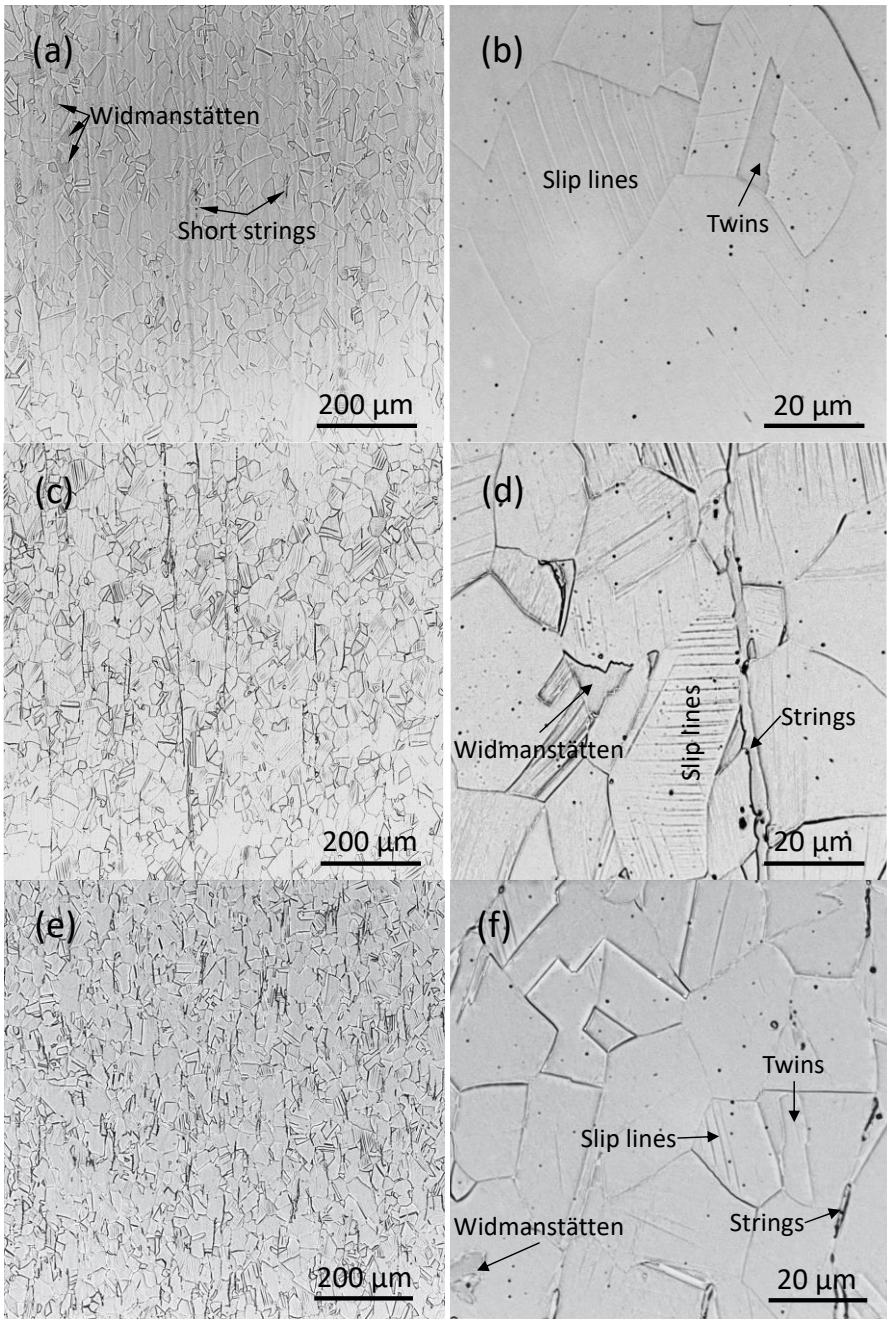

Figure 8. Optical micrographs of 15%CW 316L (N5B8): (a-b) prior to aging and aged at 350°C for (c-d) 12.5 kh and (e-f) 37 kh.

4. AGING-INDUCED CHANGES IN MECHANICAL PROPERTIES

4.1 MICROHARDNESS

The Vickers hardness results of Grade 92 (011448), 316L (T1103), and 316L (N5B8) under the conditions prior to aging and after aging at 350°C for 12.5–12.7 kh and 36–37 kh are shown in Figure 9. The 15%CW applied to 316L resulted in large standard deviations, which are reduced after aging, indicating the aging led to some local stress relaxation. The aging slightly reduced the hardness of Grade 92 with the increase of the aging time, which seems to be stabilized at ~220 HV1. In contrast, the hardness of 316L heats followed the same trend with a noticeable reduction by ~30 HV1 after the 37 kh aging, but it is still significantly (~78 HV1) higher than the hardness of the solution-annealed 316L (dashed lines in Figure 9). The hardness of 316L (T1103) samples are generally slightly lower than that of 316L (N5B8).

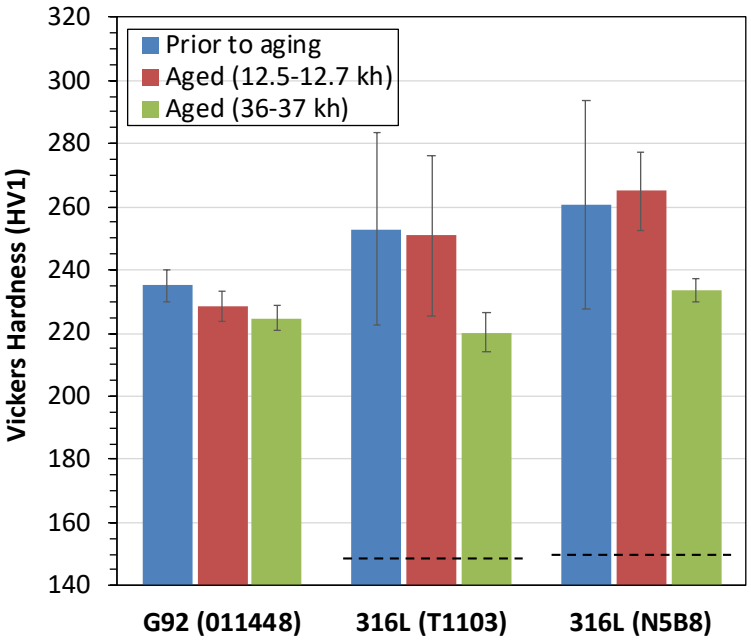

Figure 9. Vickers hardness results comparison of Grade 92 (#011448), 316L (#T1103), and 316L (#N5B8) between the prior to aging and aged at 350°C for 12.7 kh (G92), 12.5 kh (316L), 36 kh (G92), and 37 kh (316L). The 316L was subjected to 15% cold work. The dashed lines indicate the initial Vickers hardness of the solution-annealed state of 316L.

4.2 TENSILE PROPERTIES

The stress-strain curves of the tensile-tested samples of Grade 92 and the two heats of 316L aged at 350°C for 36-37 kh are shown in Figure 10. The curves show a general effect of testing temperature on the three steels, i.e., reduced strength with the increasing test temperature.

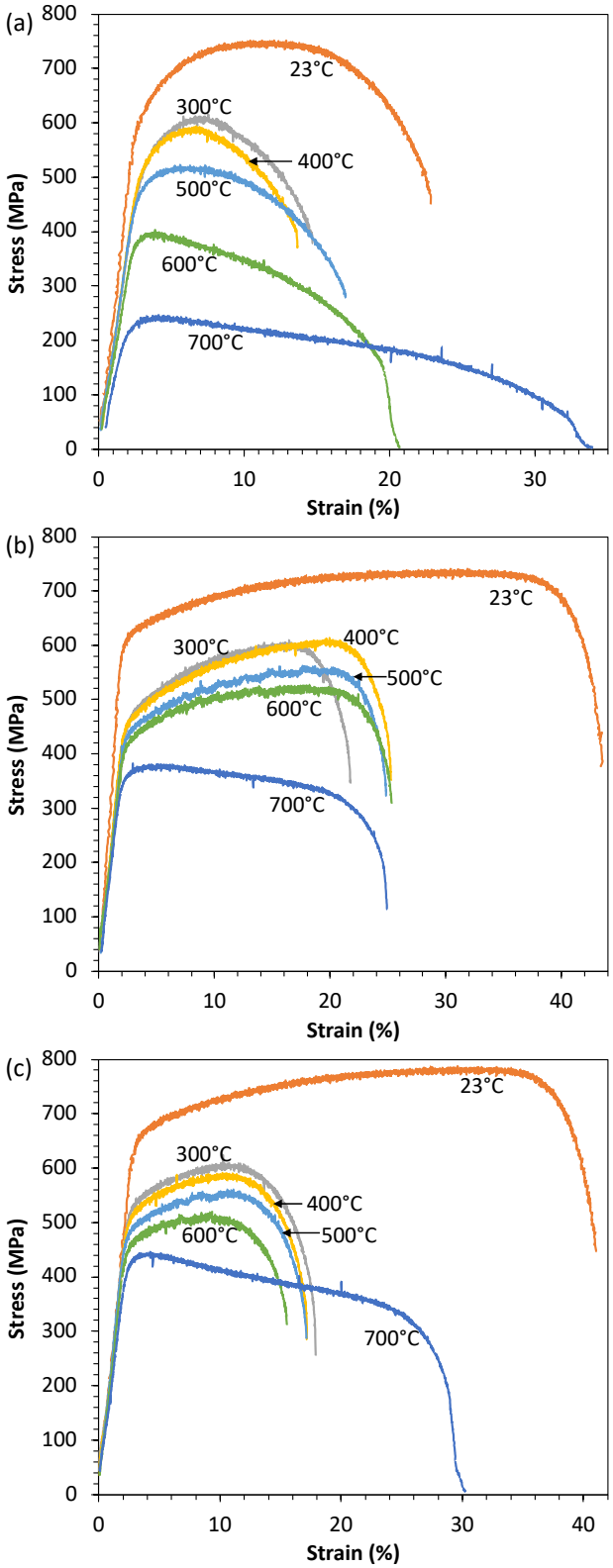

Figure 10. Tensile curves of (a) Grade 92 aged at 350°C for 36 kh, (b) 15%CW 316L (T1103) aged at 350°C for 37 kh, and (c) 15%CW 316L (N5B8) aged at 350°C for 37 kh.

The tensile properties, i.e., yield strength, ultimate tensile strength, uniform plastic elongation, and total plastic elongation, were analyzed from the stress-strain curves and compared with the unaged and shorter time aged conditions. Figure 11 shows the results of Grade 92. The 350°C aging resulted in noticeable reductions in yield and ultimate tensile strength by ~50–140 MPa at testing temperatures below 500°C. The shorter time aging, i.e., 12.7 kh, approximately reached a plateau of the strength. The 350°C aging generally increased the uniform and total plastic elongation. Several samples, however, have elongation deviated from the trend, e.g., the uniform plastic elongation of the 36 kh aged sample tested at 400°C, which may indicate the presence of "defects" in the SS-3 specimen, deteriorating the elongation results. Repeating these tests to obtain meaningful statistics are needed for more conclusive results.

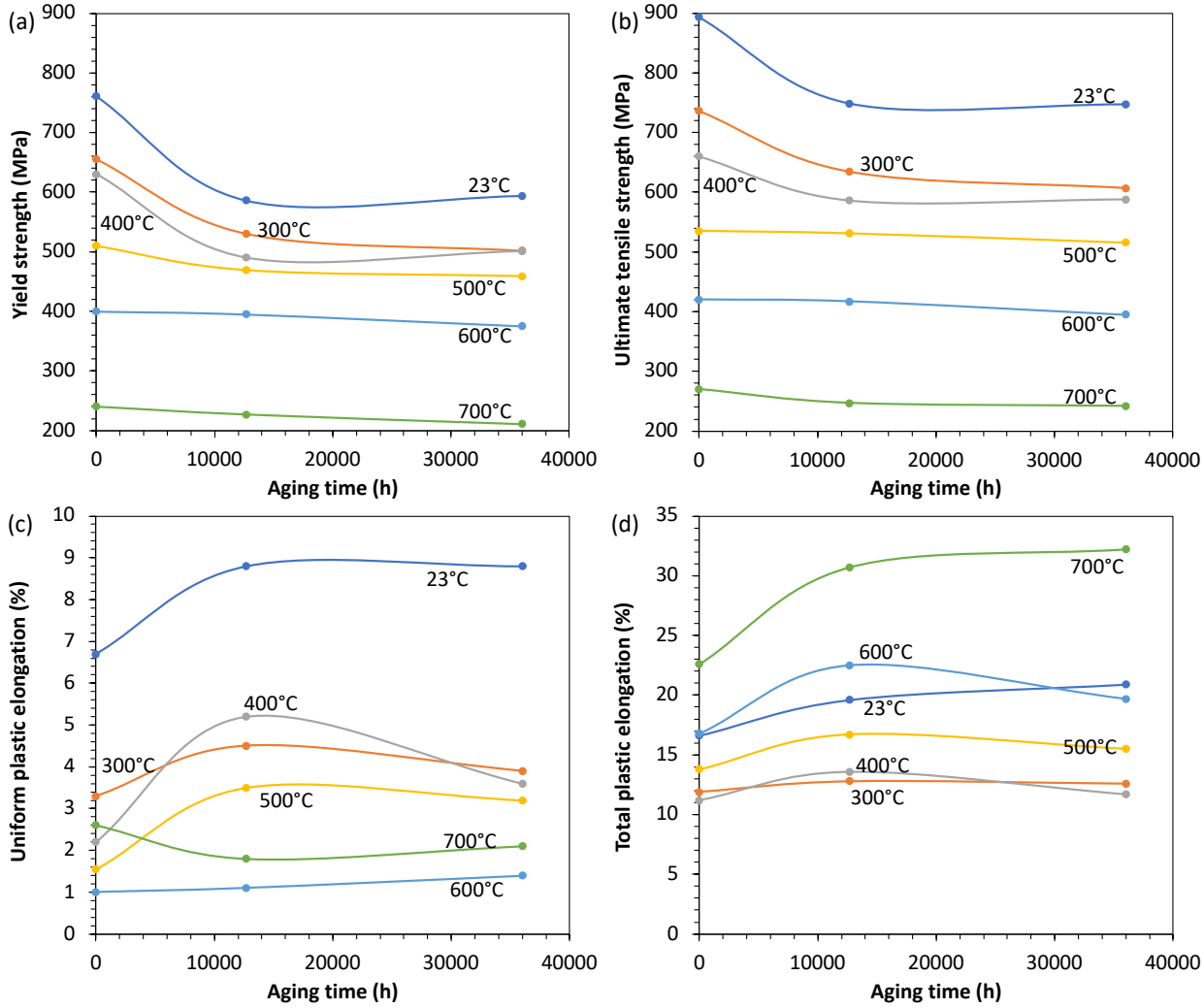

Figure 11. Effect of aging time at 350°C on (a) yield strength, (b) ultimate tensile strength, (c) uniform plastic elongation, and (d) total plastic elongation of Grade 92.

Figure 12 shows the results of 15%CW 316L (heat T1103). The 350°C aging generally resulted in reductions in yield and ultimate tensile strength at all the testing temperatures. The strength at 23, 500, and 600°C shows some variations, which might be attributable to the inhomogeneous microstructures developed in the 15%CW condition as indicated by the large standard deviations in hardness (Fig. 9). The

shorter time (12.6 kh) aging noticeably reduced the uniform and total plastic elongation while the longer time (37 kh) aging recovered the elongation to near the unaged condition.

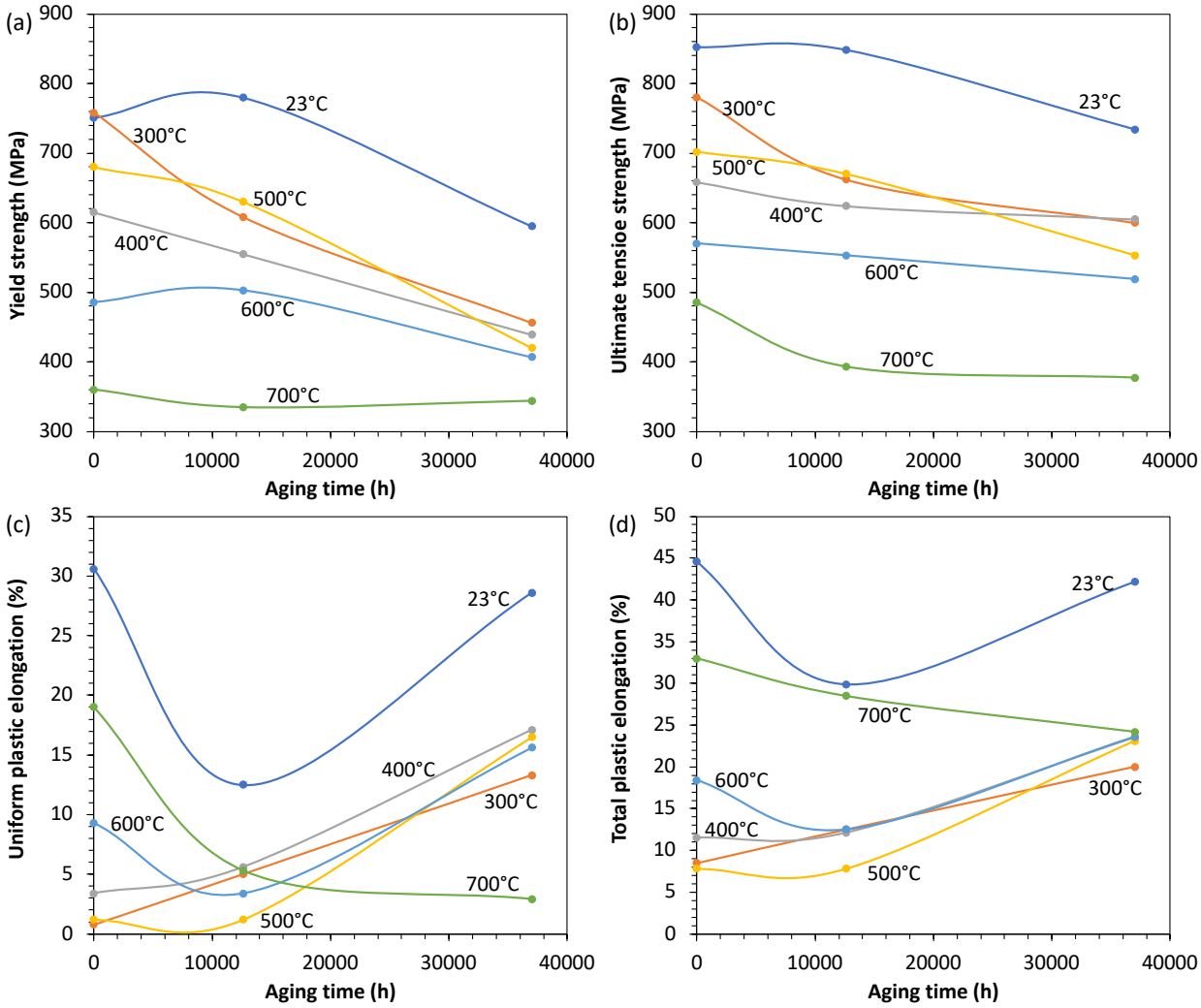

Figure 12. Effect of aging time at 350°C on (a) yield strength, (b) ultimate tensile strength, (c) uniform plastic elongation, and (d) total plastic elongation of 15%CW 316L (T1103).

Similarly, Figure 13 displays the results of 15%CW 316L (heat N5B8). The 350°C aging resulted in reductions in yield and ultimate tensile strength in general, except for the shorter time (12.5 kh) aged specimens tested at 300 and 400°C. It may reflect the inhomogeneous microstructure of the material. Unlike the aging effect on strength, the aging showed minor effects on the uniform and total plastic elongation. Except for the uniform plastic elongation above 25% at 23°C, the uniform plastic elongation values are all below 10% at elevated temperatures. Moreover, except for 23 and 700°C, the total plastic elongation values are all below ~15% at the 300–600°C.

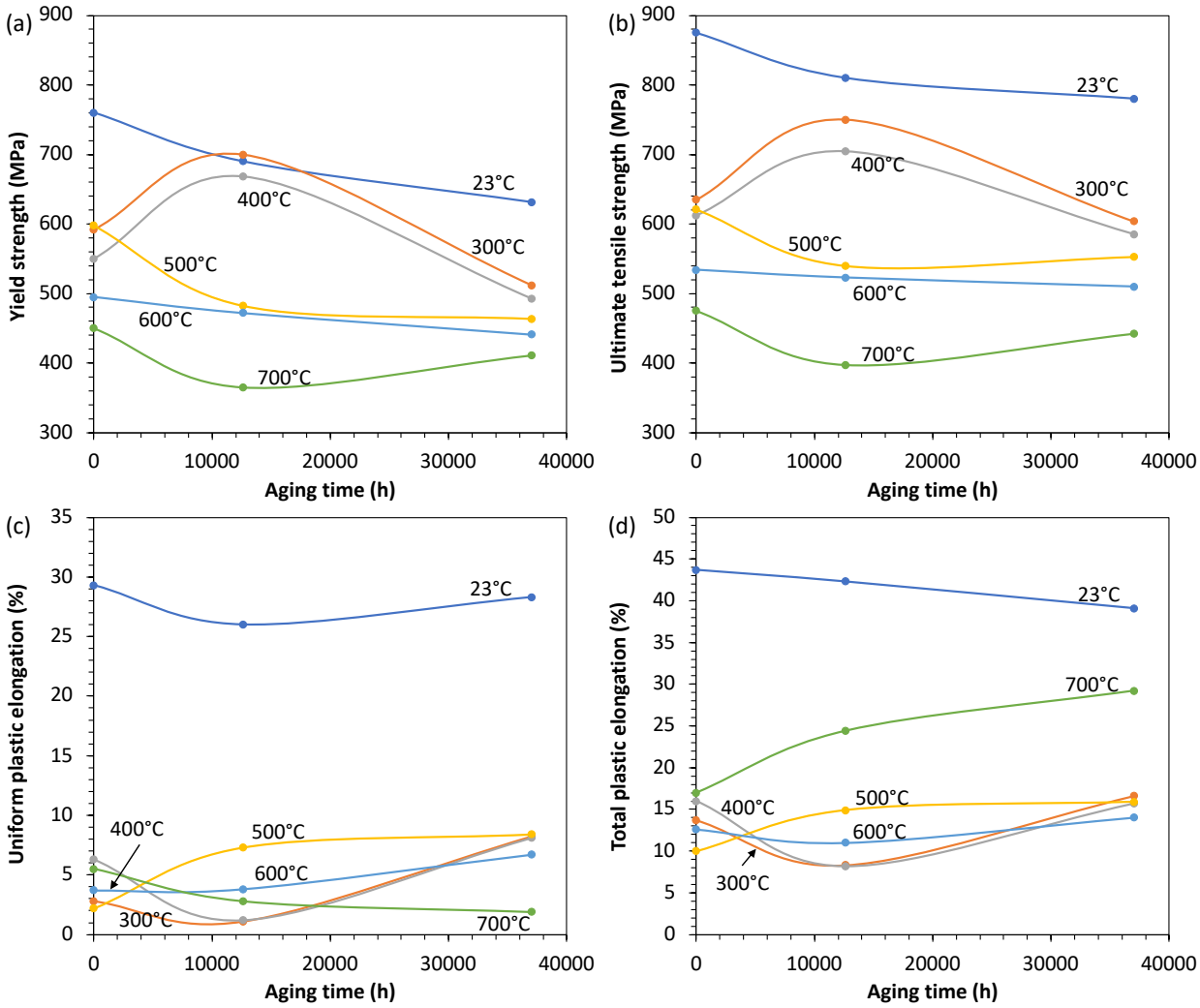

Figure 13. Effect of aging time at 350°C on (a) yield strength, (b) ultimate tensile strength, (c) uniform plastic elongation, and (d) total plastic elongation of 15%CW 316L (N5B8).

4.3 CHARPY IMPACT TOUGHNESS

The Charpy impact test results of the aged Grade 92 specimens compared with the unaged results are shown in Figure 14. To obtain DBTT and USE, impact energy-temperature curves were generated by fitting the data with a hyperbolic tangent function $E = a + b \tanh[(T - T_0)/c]$, where T is test temperature and a, b, c and T_0 are regression coefficients. In this study, T_0 is the mathematical DBTT, corresponding to the mean value of USE and lower-shelf energy (LSE), i.e., 1/2USE assuming LSE = 0 in this study. Figure 14 shows that the aged Grade 92 specimens have generally higher absorbed impact energies than the unaged condition, which lead to a higher USE by ~4 J and a lower DBTT by 20.5°C for the 12.7kh-aged condition and by ~26 J and a lower DBTT by 3.4°C for the 36kh-aged condition compared with the unaged condition. Unlike the mathematical DBTT, engineering DBTT is usually determined at a threshold absorbed energy and thus the engineering DBTT tends to decrease with an increased aging time at 350°C. The improved impact toughness with the aging time of Grade 92 at 350°C likely benefited from the reduced yield strength with increased elongation at room temperature as shown in Figure 11. The

aging induced Laves phase as shown in Figure 6 did not impair the impact toughness of the aged specimens.

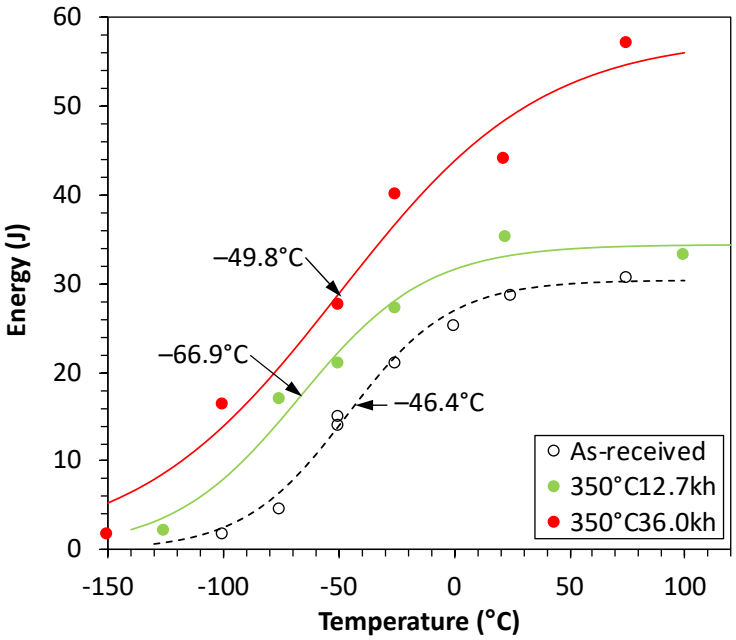

Figure 14. Temperature-dependent absorbed impact energies of the unaged and 350°C-aged (12.7 kh and 36 kh) Grade 92 specimens.

4.4 FRACTURE TOUGHNESS

Figure 15 shows the J-R curves of Grade 92, 316L-T1103, and 316L-N5B8 after thermal aging at 350°C for 36–37 kh with fracture toughness results summarized in Table 3. The analysis was performed using an automated J-R curve analysis software developed within the LWRS program based on the ASTM E1820 standard [12]. The three materials exhibited a similar temperature effect on fracture toughness (K_{Jq}) and tearing modulus. At the same temperature, 22°C or 300°C, small scattering exists in each material for fracture toughness and tearing modulus, except for one specimen of 316L-N5B8 tested at 22°C. The abnormal result of the 316L-N5B8 specimen is excluded from the data set because the fatigue precracking on this specimen was on the short side. Compared with the 22°C results, the elevated temperature at 300°C led to significant reductions in fracture toughness and minor reductions in tearing modulus in general. However, the tearing modulus of Grade 92 slightly increased at 300°C compared with 22°C. The fracture toughness of Grade 92 showed decent toughness of 289 ± 12 MPa√m with 102 ± 9 tearing modulus at 22°C, which changed to 209 ± 6 MPa√m with 111 ± 7 tearing modulus at 300°C. Comparing the two 316L heats, 316L-T1103 with ~1 vol% δ-ferrite showed noticeably higher toughness and tearing modulus than 316L-N5B8 with ~4 vol% δ-ferrite.

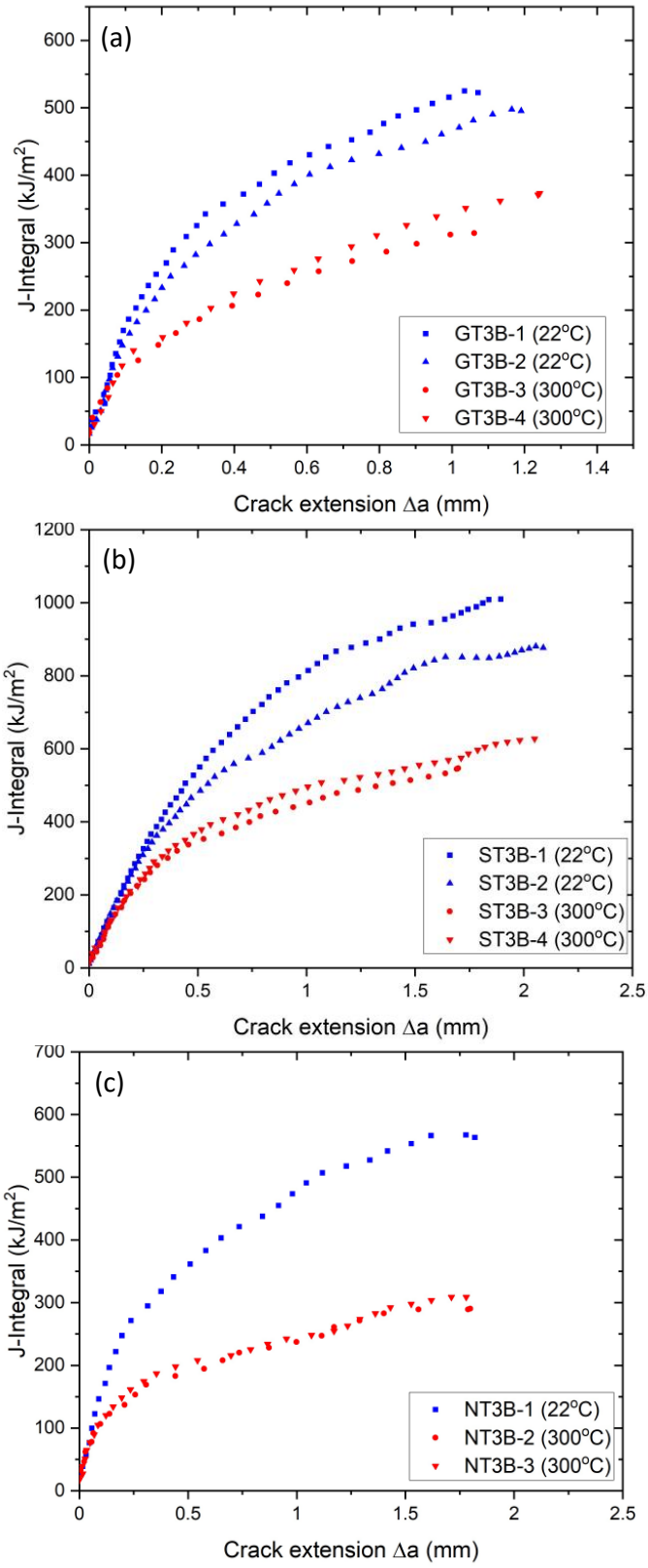

Figure 15. J-integral as a function of crack extension results of (a) Grade 92, (b) 316L-T1103, and (c) 316L-N5B8 aged at 350°C for 36–37 kh tested at room temperature and 300°C.

Table 3. Summary of fracture toughness test results of Grade 92, 316L-T1103, and 316L-N5B8 aged at 350°C for 36–37 kh.

Alloy	Specimen ID	Test temperature (°C)	Toughness K_{Jq} (MPa√m)	Average toughness (MPa√m)	Tearing modulus	Average tearing modulus
Grade 92	GT3B-1	22	297.52	289.05 ± 11.98	108.11	101.56 ± 9.26
	GT3B-2	22	280.58		95.01	
	GT3B-3	300	204.65	209.15 ± 6.36	105.58	110.76 ± 7.33
	GT3B-4	300	213.64		115.94	
316L-T1103	ST3B-1	22	395.75	371.45 ± 34.37	128.82	121.58 ± 10.24
	ST3B-2	22	347.15		114.34	
	ST3B-3	300	270.43	277.85 ± 10.49	105.58	103.82 ± 2.50
	ST3B-4	300	285.26		102.05	
316L-N5B8	NT3B-1	22	279.52	279.52	80.11	80.11
	NT3B-4★	22	322.16		104.33	
	NT3B-2	300	184.20	186.88 ± 3.79	56.99	56.11 ± 1.25
	NT3B-3	300	189.56		55.22	

★Fatigue precracking on this specimen was on the short side and therefore it might result in higher toughness than the other room temperature specimen.

Figure 16 plots the fracture toughness and tearing modulus results at room temperature and 300°C for the 12.6-12.7 kh aged samples in open circles and the 36-37 kh aged samples in solid circles for Grade 92 in black, 316L-T1103 in green, 316L-N5B8 in red. The fracture toughness and tearing modulus at 300°C data tend to be lower than that at room temperature in general. The longer aging at 350°C tends to slightly reduce or negligibly influence the fracture toughness but increase tearing modulus in general. The fracture toughness and tearing modulus of 316L-T1103 are significantly higher than that of 316L-N5B8. The fracture toughness and tearing modulus of Grade 92 are between those of the two 316L heats.

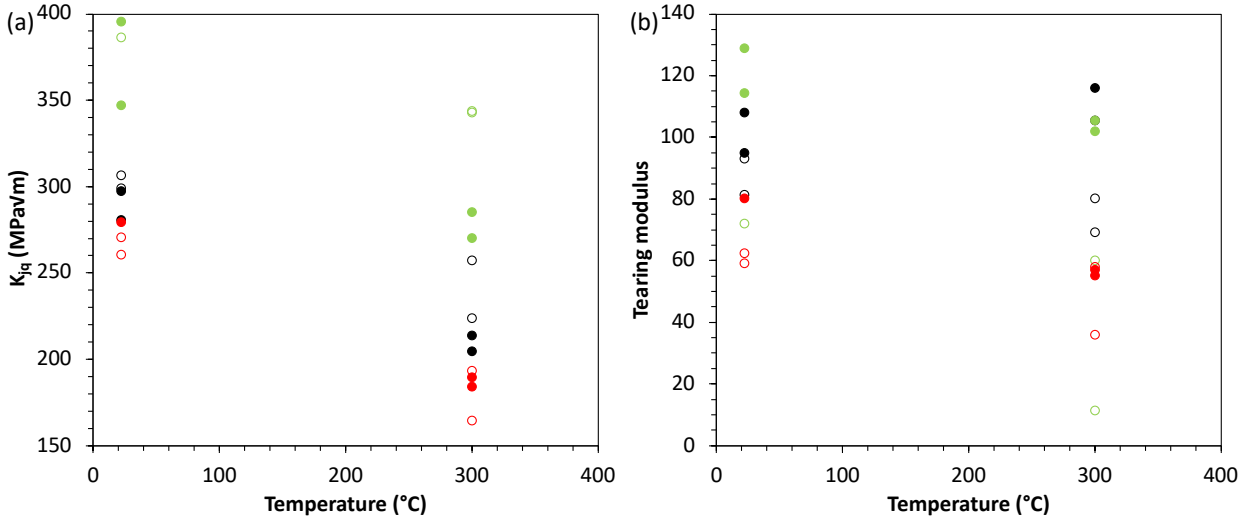

Figure 16. Room temperature and 300°C (a) fracture toughness (K_{Jq}) and (b) tearing modulus of Grade 92 (black symbols), 316L-T1103 (green symbols), and 316L-N5B8 (red symbols) aged at 350°C for 12.6-12.7 kh (open symbols) and 36-37 kh (solid symbols).

5. SUMMARY

Blocks of Grade 92 and two heats of 316L (T1103 and N5B8) were aged at 350°C for 36-37 kh. Metallographic samples, type SS-3 tensile specimens along the longitudinal direction, half-size Charpy V-notch specimens in the T-L orientation, and 0.2T or 0.25T compact tension fracture toughness specimens in the T-L orientation were machined from the aged blocks for the respective microstructural characterization and mechanical property evaluation. In general, the aging did not result in noticeable microstructural changes under optical microscopy, except for some ~100–200 nm sized Laves phase precipitates in Grade 92 under SEM.

The aging resulted in some reduction in hardness and yield/ultimate tensile strength with some increases in the uniform and total plastic elongations for the 36 kh aged Grade 92, which may have enhanced the Charpy impact toughness, e.g., ~56 J upper-shelf energy of the 36 kh aged condition compared with ~34 J of the 12.7 kh aged condition and ~30 J of the unaged condition. The fracture toughness of the 36 kh aged Grade 92 showed decent toughness of ~289 MPa$\sqrt{m}$ (K_{jq}) with ~102 tearing modulus at 22°C and ~209 MPa$\sqrt{m}$ with ~111 tearing modulus at 300°C, which slightly reduced in fracture toughness but slightly increased in tearing modulus from the ~12.7 kh aged condition. The aging induced Laves phase did not have a noticeable influence on the mechanical properties of the Grade 92 specimens.

Unlike the negligible or slight increased hardness in the ~12.6 kh aged condition, the ~37 kh aging resulted in significant reductions in hardness of 316L-T1103 and 316L-N5B8. The ~37 kh aging also significantly reduced the standard deviations of the two 316L heats, suggesting that the longer aging time reduced the 15%CW induced inhomogeneity in microstructures. The aging-induced hardness evolution is consistent with their yield strength changes. The shorter time (~12.6 kh) aging noticeably reduced the uniform and total plastic elongation while the longer time (~37 kh) aging recovered the elongation to near the unaged condition of 316L-T1103. In contrast, the aging showed minor effects on the uniform and total plastic elongation of 316L-N5B8 with similar or lower elongations than 316L-T1103. The fracture toughness and tearing modulus at 300°C in general tend to be lower than that at room temperature. The longer aging (~37 kh) at 350°C tends to slightly reduce or negligibly influence the fracture toughness but increase tearing modulus in general than the shorter aging (~12.6 kh). The fracture toughness and tearing modulus of 316L-T1103 are significantly higher than that of 316L-N5B8. The results indicate that the presence of high volume of δ-ferrite (316-N5B8) would noticeably impair fracture toughness although it may negligibly influence hardness and tensile properties. The fracture toughness and tearing modulus of Grade 92 are between those of the two 316L heats.

REFERENCES

[1] E.A. Kenik, J.T. Busby, Radiation-induced degradation of stainless steel light water reactor internals, Mater. Sci. Eng. R 73 (2012) 67–83.

[2] F.A. Garner, Radiation damage in austenitic steels, in: R.J.M. Konings, T.R. Allen, R.E. Stoller, S. Yamanaka, Comprehensive Nuclear Materials, Elsevier, The Netherlands, 2012.

[3] L. Tan, R.E. Stoller, K.G. Field, Y. Yang, H. Nam, D. Morgan, B.D. Wirth, M.N. Gussev, J.T. Busby, Microstructural evolution of type 304 and 316 stainless steels under neutron irradiation at LWR relevant conditions, JOM 68 (2016) 517–529.

[4] Critical Issues Report and Roadmap for the Advanced Radiation-Resistant Materials Program, EPRI, Palo Alto, CA and the U.S. Department of Energy, Washington, DC: 2012. 1026482.

[5] L. Tan, D.T. Hoelzer, J.T. Busby, Microstructure and basic mechanical properties of the procured advanced alloys for the advanced radiation resistant materials program, ORNL/TM-2014/439, September 22, 2014.

[6] L. Tan, B.A. Pint, High-temperature steam oxidation testing of select advanced replacement alloys for potential core internals, ORNL/TM-2017/228, May 19, 2017.

[7] X. Chen, L. Tan, Fracture toughness evaluation of select advanced replacement alloys for LWR core internals, ORNL/TM-2017/377, August 25, 2017.

[8] L. Tan, B.A. Pint, X. Chen, Toughness and high-temperature steam oxidation evaluations of advanced alloys for core internals, ORNL/TM-2016/371, September 16, 2016.

[9] L. Tan, T. Chen, B.A. Pint, Steam oxidation behavior of Ni-base superalloys 690, 725 and X-750 at 600 and 650°C, Corrosion Science 157 (2019) 487–497.

[10] D.W. Sandusky, M. Morra, J.L. Nelson, Guidelines for material procurements for use in light water reactor environments, 2015 Technical Report 3002005623, Electric Power Research Institute, September 2015.

[11] L. Tan, X. Chen, Intermediate-term thermal aging effect evaluation for Grade 92 and 316L at the LWR relevant temperature, ORNL/TM-2020/1754, September 30, 2020.

[12] A.E. Linares, L. Clowers, X. Chen, M.A. Sokolov, R.K. Nanstad, Using automated J-R curve analysis software to simplify testing and save time, Adv. Mater. Processes 177 (2019) 27.